Simulation of laser induced desorption of NO from NiO(100)

C. Bach[1], T. Klüner[2], A. Groß[1]
[1] *Physik-Department T30, Technische Universität München, 85747 Garching, Germany*
[2] *Fritz-Haber-Institut, Faradayweg 4–6, 14195 Berlin, Germany*
(Dated: April 30, 2003)

We have implemented a mixed quantum-classical scheme for the simulation of the laser-induced desorption from surfaces. This method allows a multidimensional simulation of the desorption process on realistic time scales. Using *ab initio* derived potential energy surfaces, we compare the mixed quantum-classical scheme to jumping wave-packet calculations for the laser-induced desorption of NO from NiO(100). Our results demonstrate the significant role of the multidimensionality in the desorption process, in particular the importance of surface recoil processes.

PACS numbers: 82.20.Gk, 82.20.Wt
Keywords:

I. INTRODUCTION

In recent years photochemical reactions on surfaces have received a great deal of attention, especially from an experimental point of view [1]. New technologies allowed to perform state resolved experiments which provided a unprecedented amount of information about the processes involved. The theoretical description of such reactions is still far behind. Part of the difficulties in modeling of such processes result from the fact that the Born-Oppenheimer approximation is explictly violated so that the dynamics of both electrons and nuclei have to be taken into account. Therefore, most dynamical simulations of photo-induced reactions at surfaces are limited to low-dimensional treatments with only a limited number of molecular degrees of freedom taken into account [2].

However, dynamical simulations of processes at surfaces have demonstrated the importance of a realistic multidimensional treatment [3–6]. Furthermore, quantum effects in the motion of atoms can often be neglected, in particular for atoms heavier than hydrogen, but sometimes even in the hydrogen dynamics [7, 8]. We have recently implemented, as a mixed quantum-classical scheme, the fewest switches algorithm [9] for the description of reactions at surfaces [10, 11]. In this elegant surface-hopping method, the motion of the nuclei is described classically while the dynamics of the electrons is treated quantum mechanically. The feedback between quantum and classical degrees of freedom is taken into account self-consistently by state switches whose number is minimized under the constraint of maintaining the correct statistical population of each state.

We have now extended this algorithm in order to address photo-induced reactions at surfaces. Combining ideas of previous treatments [9, 12–14], we have in particular introduced an optical potential in order to simulate the electronic system of the substrate. Due to the computational efficiency of the mixed quantum-classical method, we are able to perform multidimensional simulations of the laser-induced desorption on realistic timescales.

As a first example, we have applied our method to the laser-induced desorption of NO from a NiO(100) surface [15, 16]. In order to establish the validity of our mixed quantum-classical scheme, we have compared mixed quantum-classical two-dimensional simulations with corresponding jumping wave-packet calculations [17] on the same potential energy surface derived from quantum chemical calculations. Using the same propagation times, we obtain good agreement with the wave-packet calculations [17]. However, our simulations show that it is important to perform the dynamical simulations for sufficiently long run times. We have then extended the *ab initio* potential energy surface [17, 18] in order to take into account all NO molecular degrees of freedom plus one surface oscillator coordinate by a suitable choice of a model potential. The simulations indicate the importance of multidimensionality effects, in particular surface recoil effects, on the desorption dynamics.

II. THEORY

A. Model

The photo-induced desorption of NO from NiO has been proposed [15] to be an indirect process with an intermediate charge transfer state. This process can be viewed as a five step process (see Fig. 1): The creation of hot electrons in the substrate due to the laser irradiation (1) is followed by the transfer of one electron from a substrate state into an adsorbate state (2). Now the adsorbed molecule is accelerated away from the ground state minimum (3) and after the return of the electron into the substrate (4) the adsorbed molecule eventually desorbs if it gained enough energy in the excited state (5). There is experimental evidence that direct excitations also play a role [19]. They can be treated in an identical scheme but starting directly at step 2. Since the linear dependence of the desorption yield on the laser fluency [20] leads to the exclusion of multiple excitations in most simulations only steps 3 to 5 are explicitly treated.

To model such a process we combine ideas from Tully's fewest switching algorithm [9] and generalized surface

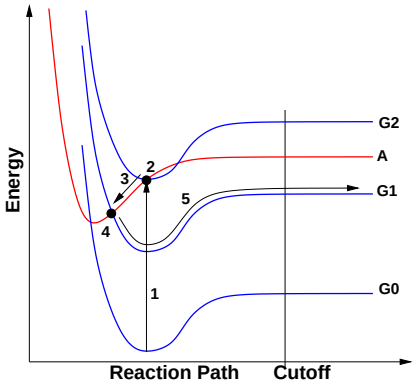

FIG. 1: Schematic drawing of a DIET process. The potential curves labeled G0–G2 correspond to the adsorbate ground state with different substrate excitations, while the curve labeled A corresponds to an excitation of the adsorbate. The numbers 1–5 indicate the five steps of the desorption process.

hopping method [12] with those of Brenig [13] and Saalfrank [14]. First we separate the nuclear from the electronic degrees of freedom, i.e. the Hamilton operator H is split into the kinetic energy T_R of the nuclear coordinates R and an electronic part H_e depending on the electronic coordinates r and parametrically on the position of the nuclei R.

$$H(r,R) = T_R + H_e(r,R) \tag{1}$$

The electronic wave function Φ is expanded into the explicitly treated excited adsorbate states ϕ_i and a collective state ψ containing the molecular ground state together with the continuum of substrate excitations.

$$\Phi(r,R,t) = \sum_i c_i(t)\phi_i(r,R) + \psi(r,R,t)$$

The influence of the collective state ψ can be taken into account by an effective non-Hermitian Hamiltonian (see chapter 16 in [21])

$$H_{eff}(r,R) = T_e + V_{eff}(r,R) + i\Delta(r,R) \tag{2}$$

where T_e is the kinetic energy operator for the electrons. The effective potential V_{eff} and the optical potential Δ are real functions of r and R. In a Newns-Andersson picture Δ is related to the lifetime broadening of a resonance state which can be determined via [22]

$$\Delta(E) \;=\; \pi \sum_{\mathbf{k}} |V_{\mathbf{k}}|^2 \delta(E - \varepsilon_{\mathbf{k}}) \tag{3}$$

With the effective Hamiltonian and a diabatic (i.e. $\nabla_R \phi_i = 0$) representation of the wave functions ϕ_i the electronic Schrödinger equation has the following form

$$\dot{c}_j = -\frac{i}{\hbar}\sum_i c_i V_{ji} + \frac{1}{\hbar}\sum_i c_i \Delta_{ji}, \tag{4}$$

where the matrix elements V_{ij} and Δ_{ji} are defined as

$$\begin{aligned} V_{ji} &\equiv \langle\phi_j|T_e + V_{eff}(r,R)|\phi_i\rangle \\ \Delta_{ji} &\equiv \langle\phi_j|\Delta(r,R)|\phi_i\rangle \;, \end{aligned} \tag{5}$$

respectively. For the diagonal elements of the density matrix $a_{ji} \equiv c_j^\star c_i$ this leads to

$$\dot{a}_{jj} = \sum_i b_{ji} + \sum_i \frac{2}{\hbar}\Re\left[a_{ji}\Delta_{ji}\right], \tag{6}$$

with $b_{ji} \equiv \frac{2}{\hbar}\Im\left[a_{ji}V_{ji}\right]$. Note that for a normalized wave function Φ the occupation probability a_{cc} for the "rest" is simply given by $a_{cc} \equiv 1 - \sum_j a_{jj}$ leading to

$$\dot{a}_{cc} = -\sum_j \dot{a}_{jj} = -\frac{2}{\hbar}\sum_{ij}\Re\left[a_{ji}\Delta_{ji}\right], \tag{7}$$

since $\sum_{ji} b_{ji} = 0$. The nuclear coordinates R are treated classically and obey the Newtonian equation of motion

$$\ddot{R} = \frac{-1}{M}\nabla\left[\frac{\langle\psi_{occ}|H_e|\psi_{occ}\rangle}{\langle\psi_{occ}|\psi_{occ}\rangle}\right], \tag{8}$$

where ψ_{occ} is the currently occupied state. Using classical equations of motion for the nuclei is a reasonable approximation as long as hydrogen is not involved.

These equations are equivalent to the ones that have been derived in the generalized surface hopping method [12]. In our scenario, however, upon a transition to the continuum state we assume that the whole excess energy is taken up by the substrate electrons, as it is usually done in the modeling of laser-induced desorption [2]. This means that upon a switch to the continuum state we just make a Franck-Condon transition, i.e. we transfer the molecule to the ground state potential with its kinetic energy preserved and perform ordinary Born-Oppenheimer molecular dynamics until the final fate of the molecule has been determined.

If just one electronically excited state is considered, then the equations become much simpler. According to Eqs. 6 and 7, the deexcitation rate is directly given by

$$\dot{a}_{11} \;=\; -\dot{a}_{cc} \;=\; \dot{c}_1 c_1^* + c_1\dot{c}_1^* = \frac{2a_{11}\Delta}{\hbar}. \tag{9}$$

In fact, for such a situation no electronic Schrödinger equation has to be numerically integrated.

Our method could in principle also be extended in order to include the excitation process. Furthermore, taking explicit time dependence into account is also straightforward. This could be used, e.g., to model the pulse shape of the exciting laser or the thermalization of hot electrons in the case of an indirect process.

B. Procedure

We start our trajectories by assuming that they have been transfered to the excited state potential in a Franck-Condon transition. The initial conditions correspond to

a Gaussian distribution in position and momentum according to the curvature of the ground state potential energy surface at the energy minimum position.

Then we numerically solve the classical equation of motion on the excited state potential. After each integration step in the excited state we decide by comparing the decay probability $p = \frac{2\Delta(R)dt}{\hbar}$ with a random number, whether to continue in the excited or the ground state. After the Franck-Condon transition to the ground state has been performed, the classical trajectory on the ground state potential is continued until it is either considered to remain trapped or until it reaches a certain cutoff distance z_{CO} from the surface in which case it is considered to be desorbed. Reaction probabilities are finally obtained by averaging over at least 10^6 trajectories.

For constant optical potential Δ this procedure is equivalent to the Gadzuk scheme [23]) as used, e.g., in [17]. In this scheme, the overall result is obtained by running jumping wave-packet calculations with different residence times and then determining an average with the weighting function $w_\tau(t) = \frac{1}{\tau}\exp(-t/\tau)$. The average residence time τ is an adjustable parameter that is directly related to a constant optical potential by

$$\tau = \frac{\hbar}{2\Delta}. \tag{10}$$

C. Potentials

The potential energy surfaces we used in our simulation are based on two two-dimensional potentials V_{ai} from Klüner et al. [17]. One corresponds to the electronic ground state while the other is a charge transfer state in which an electron from the substrate is transfered to an adsorbate state. These potentials were obtained by fitting analytical expressions to quantum chemical *ab initio* calculations. The two degrees of freedom considered are the molecule-surface distance z and the polar angle θ of the molecule with respect to the surface normal.

The other four NO degrees of freedom were additionally taken into account using a physically reasonable model potential. Details of the parametrization will be published elsewhere. Furthermore, in order to model recoil effects of the substrate we coupled a surface oscillator with coordinate s to the molecular potentials via

$$V^i_{\mathrm{N}+osc}(s,z,X) = V^i_{\mathrm{N}}(z-s,X) + V_{\mathrm{osc}}(s) \tag{11}$$

$$V_{\mathrm{osc}}(s) = \frac{1}{2} m_{\mathrm{osc}}\,\omega^2_{\mathrm{osc}}\,s^2\ , \tag{12}$$

where X stands for all other coordinates, and the upper index i is either g or e, indicating the ground or the excited state, respectively. The mass of the oscillator is taken equal to the mass of a Ni atom (58 amu) since NO is adsorbed on top of a Ni atom. The oscillator frequency has been chosen to correspond to the average value of a Debye spectrum, as it is usually done in simulations using the surface oscillator model [24]. The Debye temperature of NiO has been estimated to be between 500 and 600 K [25]. Accordingly, we have set the oscillator frequency to $\hbar\omega = 27$ meV. Anyway, the effect of the surface oscillator on the desorption dynamics is not very sensitive to the particular choice of the frequency. In the following we will report results of 2D and 6D simulations without and with the surface oscillator, denoted by 2D, 3D, 6D, or 7D calculations, respectively.

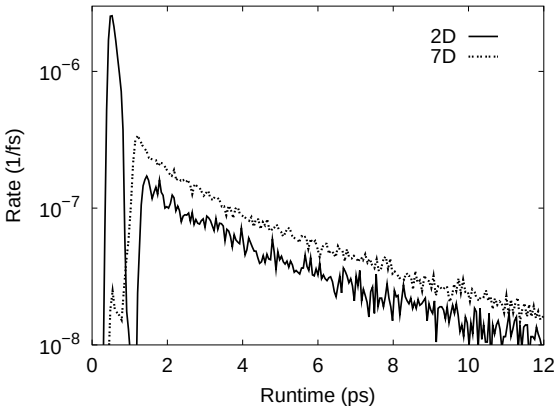

FIG. 2: Desorption rate as a function of time (excitation at time $t = 0$) in the two-dimensional (solid line) and the seven-dimensional simulations (dash-dotted line). The 2D results have been obtained with a cutoff distance of $z_{\mathrm{CO}} = 12.5$ a.u. while in the 7D calculations $z_{\mathrm{CO}} = 16.0$ a.u. has been chosen.

III. RESULTS AND DISCUSSION

In order to validate our method, we first tried to reproduce the two-dimensional wave packet results of Klüner et al. [17] using exactly the same potential. We performed both classical simulations within the Gadzuk-Scheme with the same average residence time of 24.19fs (= 1000 a.u.) as used in the wave-packet calculations as well as our proposed mixed quantum-classical scheme with the corresponding constant optical potential. Both types of simulations treat the nuclear motion classically; in fact, they yielded identical results for the desorption probabilities within the numerical accuracy, as they should. However, the mixed quantum-classical scheme with the optical potential is conceptual simpler and more flexible than the Gadzuk scheme since it does not require averaging over different residence times and it allows modeling of spatially non-constant deexcitation rates.

As for the comparison with the jumping wave-packet calculations, we obtained a larger desorption yield of 4.8% compared to 3.3% in the wave-packet calculations [17]. This was puzzling as we expected the wave-packet calculations to give a higher yield due to desorption from the classically forbidden tails of the wave function. Closer examination of the desorption rate as a function of time helped to resolve this discrepancy. In

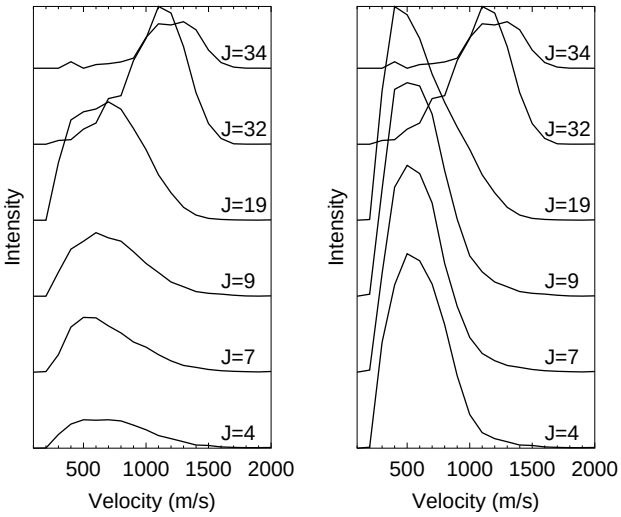

FIG. 3: Velocity distribution of desorbing molecules for various rotational quantum states. Left panel: early desorption channel; right panel: considering all desorbing molecules.

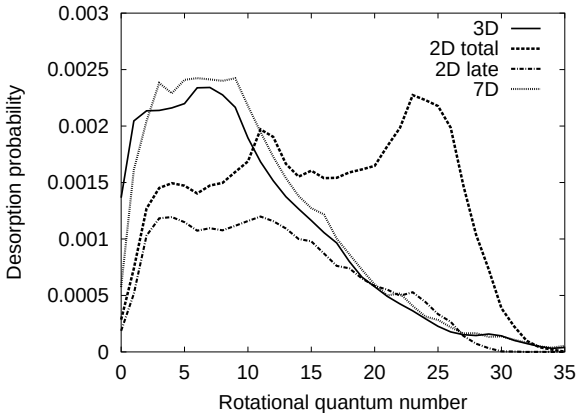

FIG. 4: Rotational distribution of desorbing molecules according to 2D, 3D and 7D calculations.

Fig. 2, we have plotted the desorption rate as a function of time for the two-dimensional (solid line) and seven-dimensional simulations (dash-dotted line). In two dimensions, there are two types of desorbing molecules. "Early" molecules that desorb within the first 1.2 picoseconds and "late" ones. The initial fast desorption peak corresponds to molecules directly desorbing after being scattered off the repulsive part of the potential. The slow trail of nearly exponentially decreasing desorption rate can be assigned to molecules being dynamically trapped [26, 27] close to the surface for a while prior to desorption.

It is apparent in Fig. 2 that the desorption rate in the 2D simulations drops to almost zero after 1.2 ps which means that the desorption probability seems to saturate after this time. The wave-packet calculations were stopped after this time due to their high computational cost. Hence the late component of the desorbing molecules were not taken into account. Due to the computational efficiency of the mixed quantum-classical scheme there were no constraints on the runtime of the trajectories. When considering only the early desorbing molecules the desorption probability is reduced to 2.93% in much better agreement with the wave-packet results. Subsequent wave-packet calculations using longer runtimes confirmed this conclusion; they yielded larger desorption yields due to the additional channel of late molecules.

The late desorption channel also shows up prominently in the velocity distribution of desorbing molecules for various rotational quantum numbers (Fig. 3). The early desorbing molecules show a rather broad velocity distribution. These distributions are in fact in a rather good agreement with the corresponding wave-packet results [17]. Taking into account also the late desorption channel leads to much narrower velocity distributions. Unfortunately, thus the agreement with the experiment [15] is reduced. In particular, the bimodal velocity distribution found in the experiment is hardly reproduced any more.

Since the mass of the substrate atoms and the NO molecule is comparable, recoil processes during the desorption process are probable. In order to include energy transfer to the substrate in the simulations, we have coupled the 2D and 6D potentials to a surface oscillator with realistic parameters, as described in the previous section. The computational costs of this extension are rather small.

In Tab. I we have collected the main results with respect to the desorption probability and the rotational temperature of desorbing molecules according to the 2D, 3D, 6D and 7D calculations. Going from 2D to 6D, i.e., including the remaining molecular degrees of freedom in the simulations, has only a small influence on the desorption distributions.

We find that the most dramatic effect comes from taking the surface oscillator into account. The total desorption probability is reduced by about 1%. Much more dramatic is the change for the early desorption channel, it is reduced by a factor of eight. This can also be seen in the desorption rate In Fig. 2), where the initial "early" peak is basically absent in the 7D results. This also affects the rotational momentum distribution. While in the 2D

	2D	3D	6D	7D
z_{CO} (a_0)	12.5	16.0	16.0	16.0
P_{des} (%)	4.84	3.63	4.74	4.02
P_{early} (%)	2.93	0.32	2.53	0.32
E_{rot} (K)	770	366	883	395

TABLE I: Desorption probabilities and mean rotational energies according to the 2D, 3D, 6D and 7D calculations. Early means desorption within the first 1.2 picoseconds.

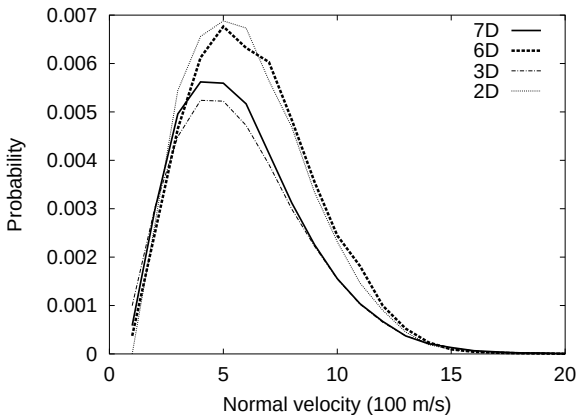

FIG. 5: Velocity distribution of desorbing molecules according to 2D, 3D, 6D and 7D calculations.

calculations we obtain a double peaked structure with a large probability for high rotational quantum numbers j, the inclusion of the surface oscillator causes the suppression of the peak at high j. The distribution is similar to that of the late molecules in the rigid surface case. This results in greatly reduced mean rotational energy in desorption, 366 K and 395 K for 3D and 7D calculations, respectively, instead of 770 K and 883 K for 2D and 6D calculations, respectively. These reduced rotational temperatures are in fact in much better agreement with experiment [15].

As far as the comparison between experiment and theory with respect to the velocity distribution is concerned, however, the agreement is greatly reduced if the late desorption channel and the surface oscillator is taken into account. In Fig. 5, we have plotted the velocity distribution according to the 2D, 3D, 6D and 7D calculations. It is fair to say that there is no indication of any bimodal velocity distribution which was found in the experiment [15] and which was also reproduced in the wave-packet calculations [17].

These findings do not necessarily imply that the conclusions of Ref. [17] with respect to the origins of the bimodality in the velocity distribution are no longer valid. In Ref. [17] it was proposed that the bimodality is a consequence of a bifurcation of the wave-packet due to the topology of the excited state potential energy surface. It might well be that this explanation is still correct. However, in the simulations only one excited charge transfer state potential out of a great number of charge transfer states [28] has been chosen. Possibly more than one excited state might be involved in the desorption process. Furthermore, the extension of the two-dimensional *ab initio* potential to seven dimensions using a physically reasonable model potential could not be realistic enough. This will be checked by mapping out higher-dimensional potential energy surfaces through quantum chemical calculations. Finally, the consideration of a spatially varying transition probability could lead to a better agreement between theory and experiment. If the deexcitation mainly occurs at specific configurations of the adsorbate, this can have a strong effect on the desorption dynamics. From a computational point of view, the simulation of such processes within our mixed quantum-classical scheme is indeed feasible and will be addressed in the future.

IV. CONCLUSION

We have implemented a mixed quantum-classical surface hopping scheme for the simulation of laser-induced desorption processes. In this method, the nuclear motion is described classically while the electrons are treated quantum mechanically. Still the feedback between nuclei and electrons is fully taken into account. In contrast to a quantum treatment the computational efficiency of our method allows a multi-dimensional treatment. We have applied this method to the laser-induced desorption of NO from NiO(100) using a previously determined *ab initio* potential energy surface. By comparing our method to jumping wave-packet calculations on exactly the same potential energy surface we verified that it is indeed justified to neglect quantum effects in the nuclear motion.

Our mixed-quantum classical method is computationally very efficient. This has allowed us to extend the simulations of the laser-induced desorption of NO from NiO(100) to longer time scales and higher dimensionalities. We find that the bimodality in the velocity distribution of desorbing molecules obtained in low-dimensional simulations vanishes if in particular surface recoil processes are taken into account. This indicates that more than one excited state might be involved in the desorption process.

[1] F. M. Zimmermann and W. Ho, Surf. Sci. Rep. **22** (1995) 127.
[2] H. Guo, P. Saalfrank, and T. Seidman, Prog. Surf. Sci. **62** (1999).
[3] A. Groß, B. Hammer, M. Scheffler, and W. Brenig, Phys. Rev. Lett. **73** (1994) 3121.
[4] A. Groß, S. Wilke, and M. Scheffler, Phys. Rev. Lett. **75** (1995) 2718.
[5] A. Groß, Surf. Sci. Rep. **32** (1998) 291.
[6] G.-J. Kroes, Prog. Surf. Sci. **60** (1999) 1.
[7] A. Groß, J. Chem. Phys. **110** (1999) 8696.
[8] Z. S. Wang, G. R. Darling, and S. Holloway, Surf. Sci. **458** (2000) 63.
[9] J. C. Tully, J. Chem. Phys. **93** (1990) 1061.
[10] C. Bach and A. Groß, Faraday Diss. **117** (2000) 99.
[11] C. Bach and A. Groß, J. Chem. Phys. **114** (2001) 6396.

[12] D. S. Sholl and J. C. Tully, J. Chem. Phys. **109** (1998).
[13] W. Brenig, Z. Phys. B **23** (1976) 361.
[14] P. Saalfrank, Chem. Phys. **193** (1995) 119.
[15] T. Mull, B. Baumeister, M. Menges, H.-J. Freund, D.Weide, C. Fischer, and P. Andersen, J. Chem. Phys. **96** (1992) 7108.
[16] G. Eichhorn, M. Richter, K. Al-Shamery, and H. Zacharias, Surf. Sci. **368** (1996) 67.
[17] T. Klüner, H.-J. Freund, V. Staemmler, and R. Kosloff, Phys. Rev. Lett. **80** (1998) 5208.
[18] T. Klüner, H.-J. Freund, J. Freitag, and V. Staemmler, J. Mol. Catal. A **119** (1997) 155.
[19] H. Zacharias, G. Eichhorn, R. Schliesing, and K. Al-Shamery, Applied Physics B **68** (1999).
[20] G. Eichhorn, M. Richter, K. Al-Shamery, and H. Zacharias, JCPhys **111** (1999).
[21] R. G. Newton, *Scattering Theory of Waves and Particles*, McGraw-Hill, 1966.
[22] R. Brako and D. M. Newns, Rep. Prog. Phys. **52** (1989) 655.
[23] J. W. Gadzuk, Surf. Sci. **342** (1995) 345.
[24] A. Groß and W. Brenig, Surf. Sci. **302** (1994) 403.
[25] K. S. Upadhyaya, G. K. Upadhyaya, and A. N. Pandey, J. Phys. Chem. Solids **63** (2002) 127.
[26] A. Groß and M. Scheffler, J. Vac. Sci. Technol. A **15** (1997) 1624.
[27] C. Crespos, H. F. Busnengo, W. Dong, and A. Salin, J. Chem. Phys. **114** (2001) 10954.
[28] T. Klüner, H.-J. Freund, J. Freitag, and V. Staemmler, J. Chem. Phys. **104** (1996) 10030.